Materials Science and Engineering, A159 (1992) 111-118

Non-destructive depth profiling of laser-processed Zr-2.5Nb alloy by IR photothermal radiometry

M. Munidasa, Ma Tian-Chi* and A. Mandelis

Photothermal and Optoelectronic Diagnostics Laboratory, Department of Mechanical Engineering, University of Toronto, Toronto, Ontario M5S 1A4 (Canada)

S. K. Brown and L. Mannik

Ontario Hydro Research Division, 800 Kipling Avenue, Toronto, Ontario M8Z 5S4 (Canada)

(Received April 13, 1992; in revised form July 6, 1992)

Abstract

A non-destructive remote sensing technique for obtaining quantitative thermal diffusivity depth profiles of near-surface inhomogeneities in opaque solids is reported. In this technique, the difference in the photothermal signal frequency response of a sample with an inhomogeneous surface layer compared with that of a homogeneous sample of the same material has been utilized. The signal was monitored by the radiometric emission from the sample surface. Applications to the inspection of laser-processed Zr-2.5Nb alloy samples are presented. Profiles obtained from this method are consistent with the profiles obtained from destructive methods such as microhardness testing.

1. Introduction

Zirconium-based alloys are often specified for engineering use in many corrosive environments because of their resistance to corrosion. A combination of good corrosion resistance, a low neutron absorption cross-section, and adequate mechanical properties has made these alloys a widely accepted cladding and structural material in water-cooled nuclear reactors. An alloy containing 2.5 wt.% Nb has been extensively used in CANDU (a trademark of Atomic Energy of Canada Ltd.) reactors for the fabrication of pressure tubes. The alloy is used either in heat-treated (quenched and aged) or in cold-worked conditions. It is known that the corrosion resistance of zirconium alloys is sensitive to microstructure and, hence, a marked improvement in the corrosion resistance can be achieved by using the appropriate heat treatment.

Laser processing of materials is of interest in many industrial applications where a surface layer is modified to obtain improved properties, such as hardness, corrosion resistance and fatigue strength, while the base material remains in the original condition. Previous research [1-4] has shown that laser processing (laser glazing, laser beta-phase heat treatment) of zirconium alloy can result in a fine-grain structure with a fine dispersion of intermetallic precipitates, which can greatly enhance corrosion resistance. When selecting and controlling the laser processing parameters to optimize surface improvement, it is very important to evaluate the effects caused by laser processing.

Thermal conductivity, which depends on the transport properties of the material, is very sensitive to the changes that take place in the material as a result of laser processing. Considering this change in thermal conductivity and the typical depths of hardened layers involved, photothermal techniques should be a good non-destructive method by which to profile these subsurface inhomogeneities. Essentially, any photothermal technique involves generating a periodic temperature distribution in the material, using a periodic heat source, such as an intensity-modulated laser beam focused onto the material surface. This periodic temperature distribution, known as a 'thermal wave', is heavily damped and has a modulation frequency-dependent penetration depth. The amplitude of these waves decreases by a factor of e^{-1} within a distance from the surface of one diffusion length, μ, given by

$$\mu = (\alpha/\pi f)^{1/2}$$

where α is the thermal diffusivity of the material and f is the modulation frequency. Thermal waves also undergo a phase lag with increasing penetration depth. Since the amplitude and the phase shift directly depend on the thermal diffusivity, depth-selective information

*On leave from Quantum-Electronics Institute, South China Normal University, Guangzhou, China.

0921-5093/92/$5.00

on this property can be obtained by measuring the amplitude and phase of thermal waves as functions of the modulation frequency. Thermal diffusivity α is related to thermal conductivity k, specific heat c and density ρ through $\alpha = k/\rho c$. Thermal waves can be detected at the surface of the solid by various techniques [5]. In this work we used the IR radiometric detection method [6] which relies on the detection of variations in the IR thermal radiation emitted from the sample surface that is excited by an intensity-modulated laser. The main advantage of radiometric detection over other photothermal monitoring techniques is its totally non-contact nature. This allows measurements to be made on samples of any shape and size, as well as on samples in hostile environments such as high temperature, high pressure or vacuum. In similar work reported earlier [7] using the gas-cell photoacoustic (PA) detection method, samples had to be of dimensions compatible with an air-tight cell. Therefore, samples had to be machined to fit the cell, and PA detection cannot be strictly non-destructive.

In earlier stages of analytical development, photothermal depth profiles of inhomogeneities in the material were approximated by a multilayer model to fit the frequency scan data [8]. This method can be applied successfully to layered materials when each layer is homogeneous. However, it was not possible to measure both the thickness and the thermal diffusivity independently [9]. Recently, a direct inversion method for arbitrarily and continuously inhomogeneous materials based on the Hamilton–Jacobi formulation of thermal wave physics has been presented [10]. This methodology has been used successfully to profile magnetic field-induced inhomogeneities 20–30 μm below the surface in liquid crystals [11] and, subsequently, with some modifications, to surface-hardened layers in laser-processed steels [7]. In this paper, we present a study of laser-processed Zr–2.5Nb alloy using the non-contact, non-destructive IR radiometric detection technique and the inversion procedure described in ref. [7].

2. Experimental procedure

A schematic diagram of the experimental apparatus is shown in Fig. 1. An Ar^+ laser (514 nm) with a modulated power up to 300 mW, modulated by an acousto-optic (A/O) modulator, is directed onto the sample surface. The radiation emitted by the sample surface is collected and focused onto the detector using off-axis parabolic mirrors [12]. The heated area of the sample surface is centred around the focal point of one mirror and the detector is at the focal point of the other mirror. The detector is a liquid-nitrogen-cooled

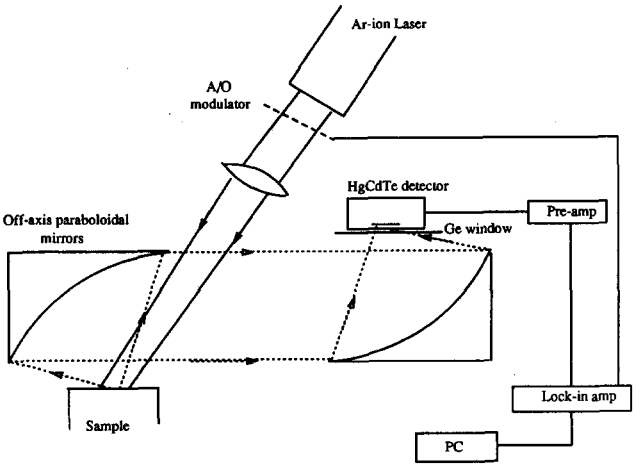

Fig. 1. Schematic diagram of the experimental set-up.

HgCdTe (EG&G Judson model J15D16-M204) with an active area of 1 mm^2 and a spectrally sensitive range of 2–24 μm. An argon-coated germanium window with a transmission bandwidth of 2–13 μm is mounted in front of the detector to block any visible radiation from the pump laser. The pump beam spot diameter on the sample is about 2 mm, which is larger than the maximum profiling depth (less than 0.5 mm) of interest. This maintains the one-dimensional heat diffusion formalism assumed in the theory. The signal, which is proportional to the change in the IR radiation emitted from an area viewed by the detector, is amplified by a preamplifier (EG&G Judson model PA-100) before being sent to the lock-in amplifier (EG&G model 5210). The lock-in amplifier's internal oscillator is used to modulate the laser beam. It is interfaced with a personal computer so that the frequency scan and the data acquisition and storage are automated.

In our reconstruction method [7], it is assumed that the detected signal is proportional to the surface temperature variation. This is not necessarily true in radiometric detection. The output voltage of an IR detector which detects a narrow spectral bandwidth, such as in our system (mostly in the 8–12 μm range), may be written as [13]

$$V = C(T + T_0)^n \tag{1}$$

where C is a constant that involves detector parameters, detection electronics and the surface emissivity of the sample, and T is the temperature excursion above the ambient temperature T_0. The exponent n in eqn. (1) is approximated by [14]

$$\begin{aligned} n &\approx 5\frac{\lambda_m}{\lambda_d} \qquad \text{for } \frac{\lambda_d}{\lambda_m} \leqslant 2.5 \\ n - 1 &\approx 2.5\frac{\lambda_m}{\lambda_d} \qquad \text{for } \frac{\lambda_d}{\lambda_m} > 2.5 \end{aligned} \tag{2}$$

where λ_m is the peak emission wavelength related to the operating temperature by Wien's law and λ_d is the centre wavelength of the detection bandwidth. If the maximum temperature elevation T is much smaller than T_0, the signal increase over the initial level V_0 (i.e. the signal detected by the lock-in) can be written (from a first-order approximation of eqn. (1)) as

$$V - V_0 = nCT_0^{n-1}T \equiv kT \tag{3}$$

showing that the detected signal is linearly proportional to the surface temperature excursion. For a given T, departure from this linearity can also occur owing to a large n value, high emissivity of the sample surface, or a large T_0. Therefore, it is necessary to test the validity of this linearity for each sample. Figure 2 shows the detected IR signal for three different samples at the lowest frequency used (corresponding to the highest temperature excursion) at different levels of modulated pump beam power. The signal from two of the samples remains linear up to 240 mW, while the other sample departs from linearity above 120 mW. The maximum possible pump beam power to be used for each sample within the linear range is determined by these curves.

Samples of Zr–2.5wt.%Nb (50 mm × 25 mm × 4 mm) were provided by the Whiteshell Laboratories of Atomic Energy of Canada Ltd. (AECL). Laser processing was performed in the Industrial Laser Laboratory at Ontario Hydro, using the full power of a 1.5 kW CO_2 laser in the TEM_{00} mode focused through a cylindrical lens to a line 8 mm × 2 mm. To avoid nitrogen contamination, the samples were processed inside a vacuum chamber. The beam scan speed was 1.7 cm s^{-1} and tracks were overlapped by 25% to achieve full coverage. One side of each sample was processed (Table 1). For one of the samples (sample no. 1) there was no surface preparation before laser processing, while the other sample (sample no. 2) was blased with 8 μm glass beads at a pressure of 20 lbf in^{-2}, to dull the surface in order to increase the absorptivity. A sample (no. 3) with glass blasting but without laser processing was also tested. Data from a fourth sample (no. 4) laser processed in an atmospheric environment (contaminated with nitrogen) which had a non-monotonic depth profile (otherwise of no interest to this laser processing work) are also presented here to show the ability of our technique to reconstruct such profiles.

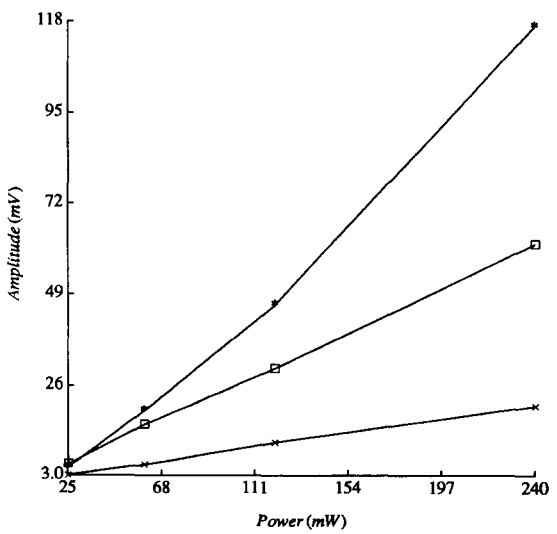

Fig. 2. Pump laser power *vs.* signal amplitude for two laser-processed samples and the reference (indicated by ×) at 22 Hz.

For each sample, photothermal radiometric (PTR) signal amplitudes and phases were recorded in the modulation frequency range between 5 Hz and 125 kHz. The frequency increment was such that it corresponds to approximately equal depth intervals with the desired resolution. The lowest frequency was limited by the preamplifier bandwidth (5 Hz–1 MHz) and the highest frequency by the lock-in amplifier range (0.5 Hz–125 kHz). For each surface, data were averaged over three experimental runs to reduce random noise. A set of data from an original Zr–2.5Nb alloy reference sample at the same frequencies was also taken for comparison. It is very important to record the reference data immediately after each surface-modified sample, to avoid any long-term instrumental drifts.

In obtaining quantitative depth profiles, it is necessary to know the thermal diffusivity of the Zr–2.5Nb reference sample. The same experimental set-up was used to measure the bulk thermal diffusivity by directing the unfocused pump beam onto the back of the sample and measuring the IR radiometric emission from the opposite surface. For this measurement, a sample 0.8 mm thick was machined to obtain a good signal-to-noise ratio. Assuming one-dimensional heat flow through the thickness of the material, the thermal diffusivity can be calculated from

TABLE 1. Description of the Zr–2.5Nb alloy samples used in this work

Sample number	Description
1	Laser processed in a vacuum using 1.5 kW CO_2 laser. No surface preparation before processing
2	Blasted with 8 μm glass beads before laser processing. Processing parameters same as sample 1.
3	Glass blasted as in sample 2 but no laser processing
4	Laser processed in air. No surface preparation before processing. Processing parameters unknown

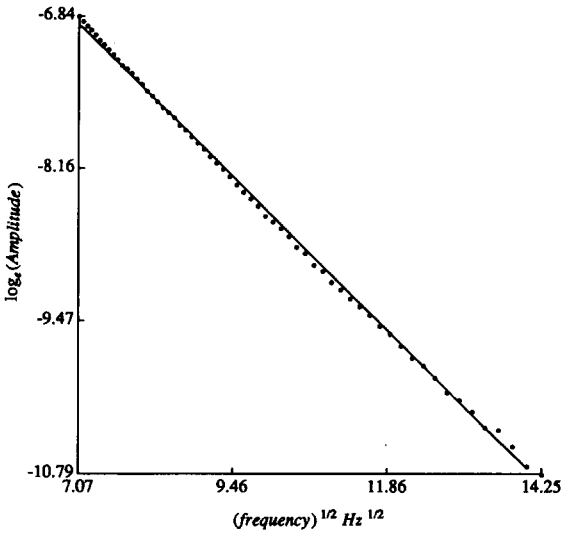

Fig. 3. A plot of $\log_e$(amplitude) *vs.* (frequency)$^{1/2}$ of the PTR signal (•) from the back surface of a Zr–2.5Nb alloy reference sample 0.8 mm thick. Solid line represents the corresponding linear fit.

the slope of a plot of $\log_e$(amplitude) or phase (in radians) *vs.* $f^{1/2}$ [15] (Fig. 3). From this technique we found the thermal diffusivity of Zr–2.5Nb to be equal to 6.2×10^{-6} m^2 s^{-1}. A literature value for this particular alloy was not available. The literature value [16] for pure zirconium is 9×10^{-6} m^2 s^{-1} and for Zircalloy-2, which is claimed [17] to have similar physical properties, it is approximately 6×10^{-6} m^2 s^{-1} [17].

To compare photothermal measurement results with the actual hardness profile, the laser-processed hardened zone was determined by cross-sectioning the sample and performing a microhardness test, using a Vickers indentor with a 100 g load. From the microhardness profile, the depth of the hardened zone was measured.

3. Results

3.1. Frequency response data

For each processed sample and its reference, the ratios of the PTR signal amplitudes were taken and the phases were subtracted. Variations in the amplitude ratio and the phase difference with frequency are related to the change in the thermal diffusivity with depth owing to processing. Frequency scan data from several different points on the same surface of the reference sample were also compared with each other to see whether there are any inhomogeneities in the material itself. These data showed the Zr–2.5Nb alloy to be homogeneous. By contrast, we have been able to observe large variations in the frequency response data from point to point in other materials, such as aluminium alloys.

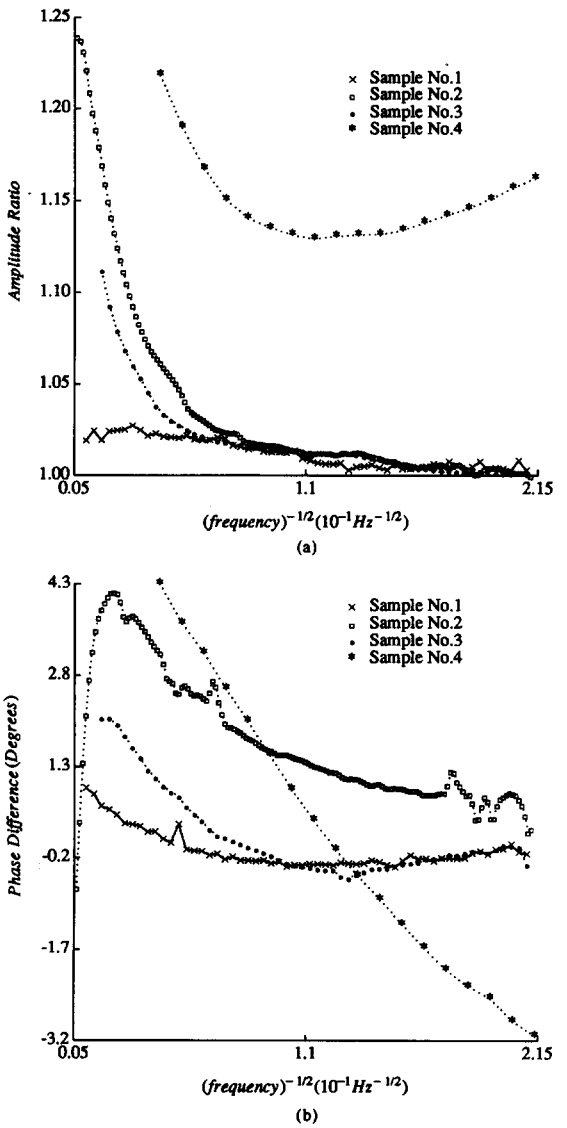

Fig. 4. PTR signal (a) amplitude ratio and (b) phase difference between samples 1, 2, 3, 4, and the unprocessed reference sample as a function of (frequency)$^{-1/2}$.

Figure 4 shows the frequency dependence of the amplitude ratio (Fig. 4(a)) and the phase difference (Fig. 4(b)) for the four samples mentioned above, each one compared with its reference. The data clearly demonstrate the difference in the signal as a result of laser processing (samples 1, 2 and 4) and glass blasting itself (sample 3). The strong dependence of the signal on the exact conditions of material processing should be noted. Figure 5 shows the corresponding microhardness profiles of the same samples. It was difficult to make reliable microhardness measurements very close to the edge (below 50 μm) of the sample cross-section. Only samples 2 and 4 show a hardened layer below a depth of 50 μm. The hardened layer of sample 2 extended to about 300 μm. Sample 4 shows a non-

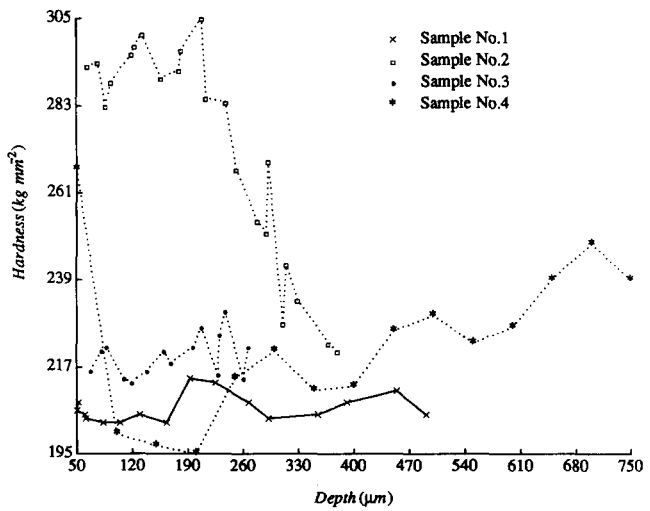

Fig. 5. Hardness obtained from the Vickers hardness test *vs.* depth for cross-sections of samples 1, 2, 3 and 4.

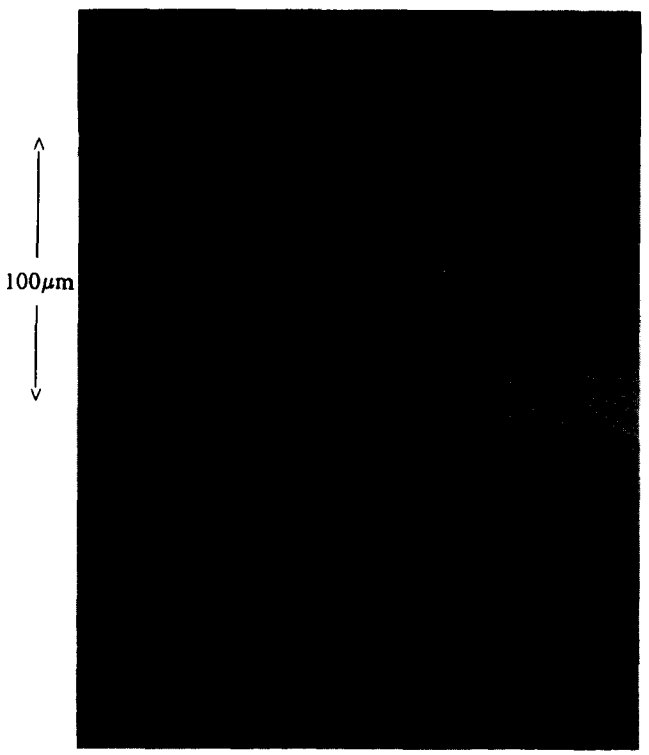

Fig. 6. Optical microscopy photograph (magnification 400×, polarized light) of the cross-section of the laser-processed layer in sample 2.

monotonic profile which extends over 1 mm (not shown). Figure 6 shows a photograph of a polished and etched cross-section of sample 2 observed under an optical microscope. A surface layer of thickness about 100 μm which was resistant to etching (corrosion) is clearly visible, and it gradually fades away towards the bulk.

3.2. *Reconstruction of thermal diffusivity profiles*

For a homogeneous metallic material, assuming (a) all the pump beam energy is absorbed at the surface and (b) the effusivity of the sample is much larger than that of surrounding air, the depth-dependent a.c. temperature $T_s(x,\omega)$ at angular modulation frequency ω given in ref. 10, eqn. (39), reduces to

$$T_s(x,\omega)=\frac{I_0\eta}{2k_s\sigma_s}\exp(-\sigma_s x)\equiv T(0,\omega)\exp(-\sigma_s x) \qquad (4)$$

where I_0 is the amplitude of the modulated optical intensity, k_s the sample thermal conductivity, σ_s the complex thermal diffusion coefficient and η the optical-to-thermal conversion efficiency averaged over the pump beam spectral bandwidth. Assuming the linear dependence given in eqn. (3), the backscattered radiometric signal $S_B(\omega)$ at the IR detector monitoring the thermal radiation from the optically opaque excited surface of a semi-infinite sample is [18]

$$S_B(\omega)=k\beta'\int_0^\infty T_s(x,\omega)\exp(-\beta' x)\,dx \qquad (5)$$

where β' is the IR absorption coefficient of the sample averaged over the detection spectral bandwidth. Substituting eqn. (4) in eqn. (5), and assuming photothermal saturation (*i.e.* IR absorption coefficient β' much greater than thermal diffusion coefficient $|\sigma_s|/2^{1/2}$)

$$S_B(\omega)=\eta kT(0,\omega) \qquad (6)$$

For an inhomogeneous sample, $T(0,\omega)$ retains its definition and the ratio of the signal $S_{Bin}(\omega)$ from the inhomogeneous sample to that from the homogeneous sample (reference) ($S_{Bref}(\omega)$) is given by

$$\frac{S_{Bin}(\omega)}{S_{Bref}(\omega)}=\frac{T_{in}(0,\omega)}{T_{ref}(0,\omega)}\equiv|M(\omega)|\exp\{i\Delta\phi(\omega)\} \qquad (7)$$

where $|M(\omega)|$ is the PTR amplitude ratio and $\Delta\phi(\omega)$ is the PTR phase difference.

In deriving eqn. (7), it has been assumed that the non-radiative conversion efficiency η and the emissivity ε of the two sample surfaces are the same. This is not necessarily true for the surface-modified samples being investigated here. The variation of these surface properties between the surface-modified sample and the reference sample leads to an amplitude ratio $|M(\omega)|$ modified by a factor equal to the $\eta\varepsilon$ ratio of the two surfaces. It is possible to eliminate this factor by dividing $|M(\omega)|$ at all frequencies by the amplitude ratio $|M(\omega_0)|$ at the lowest possible frequency $\omega_0(\omega_0/2\pi=5$ Hz in our system), provided the hardened layer thickness is much smaller than the penetration depth at ω_0. This assumption is justified if the phase difference

$\Delta\phi(\omega)$ approaches zero at ω_0, which was true for samples 1, 2 and 3. This, together with the low frequency limit of the system, sets a limit on the maximum thickness of the hardened layer that can be investigated. Microhardness test profiling for sample 4 shows that its inhomogeneity extends over 1 mm, which is beyond the penetration depth at 5 Hz. Therefore, the surface emissivity correction for this sample was obtained by comparing the data at a few frequencies with those obtained from the photoacoustic experiment [7] where the signal is affected only by η. The optical-to-thermal conversion efficiency η was calculated from the measurements of the direct pump beam power and of the reflected and scattered pump beam light from the sample surfaces; the latter were measured by replacing the IR detector with a laser power meter in the experimental system. The values of η thus obtained for sample 4 and the reference were 0.91 and 0.78 respectively.

The normalized frequency response signal for a continuously thermally inhomogeneous solid sample is given by [7]

$$|M(\omega)|\exp\{i\Delta\phi(\omega)\}=\frac{1}{R(\infty)}\left[1-\frac{1}{4}R^{1/2}(\infty)\times\exp\left\{-\frac{(1+i)\sqrt{\omega}}{2\sqrt{2q}}\frac{1}{\sqrt{\alpha_\infty}}\ln\left(\frac{\alpha_\infty}{\alpha_0}\right)\right\}\right] \tag{8}$$

where a monotonically increasing thermal diffusivity depth profile ($\alpha_\infty > \alpha_0$) of the form

$$\alpha_s=\alpha_0\left(\frac{1-D\exp(-qx)}{1-D}\right)^2 \tag{9}$$

where $D=1-(\alpha_0/\alpha_\infty)^{1/2}$, is assumed. Here, α_0 and α_∞ are thermal diffusivities at the surface ($x=0$) and in the bulk, respectively, and q determines the rate of change of $\alpha_s(x)$. In eqn. (8)

$$R(x)\equiv e_s(0)/e_s(x) \tag{10}$$

where $e_s(x)$ is the depth-dependent thermal effusivity ($e_s(x)=\{K(x)\rho(x)c(x)\}^{1/2}$) of the sample. Although eqn. (8) is valid for a monotonically increasing thermal diffusivity profile given by eqn. (9), arbitrary $\alpha_s(x)$ profiles can be handled by redefining (updating) the two constants (α_0,q) at every modulation frequency $f_j=\omega_j/2\pi$, starting with the highest frequency, using the experimental data values and assuming knowledge of the value of thermal diffusivity α_∞ of the homogeneous reference sample. It is also possible to normalize the inhomogeneous sample data by any homogeneous, optically opaque, thermally thick sample, provided its thermal diffusivity α_{ref} and the bulk thermal diffusivity α_∞ of the inhomogeneous sample are known. A complete methodology for solving the inverse problem and obtaining diffusivity depth profiles can be found elsewhere [7] and will not be repeated here. In this method of solution, it is implicitly assumed that the effusivity ratio at $x=0$ and $x=\infty$ is adequately represented by the respective conductivity ratio, so that

$$\alpha_0 \approx \alpha_\infty R^2(\infty) \tag{11}$$

However, in the actual application, its value is updated at every new frequency, so that eqn. (11) becomes readjusted from data values. As a result the impact of the approximation of eqn. (11) is negligible [10].

Figure 7 shows the thermal diffusivity depth profiles for all four samples obtained from the frequency response data using the reconstruction algorithm described above. This shows the ability of this technique to obtain profiles that reach as close as 8 μm beneath the surface where the microhardness test failed (unless it was done at the top surface, removing layer by layer). The diffusivity profile of sample 1 shows that laser processing without any surface preparation has hardly changed the material. (A slight drop in diffusivity is seen down to a depth of about 25 μm.) Sample 2 shows a monotonically decreasing diffusivity profile towards the surface, starting from a depth of about 200 μm with a faster drop starting at around 90 μm. The thermal diffusivity profile also shows a change of shape at about 20 μm. This is a reproducible feature which may be related to the transformed microstructure of the material. Optical micrograph and trans-

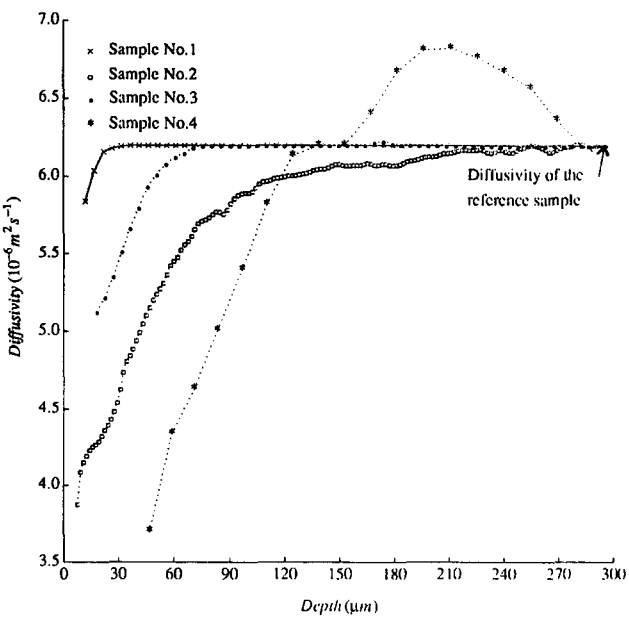

Fig. 7. Reconstructed thermal diffusivity profiles of samples 1, 2, 3 and 4.

mission electron microscopy (TEM) studies (courtesy of K. F. Amouzouvi, Whiteshell Laboratories) on this sample have shown the presence of α-Zr grains in near-surface layers less than 15 μm in depth and a martensitic structure in deeper layers down to about 100 μm. The microhardness profile for this sample (Fig. 5) shows an increase in hardness starting from a depth of about 300 μm up to 200 μm and then remains constant towards the surface. However, the hardness measurements made on the laser-processed top surface (indentation up to 5 μm) have given a much higher value (347 kg mm^{-2}) compared with the value at 50 μm (294 kg mm^{-2}). Although the shapes of the two profiles are different for sample 2, the overall trends of the inhomogeneous layer obtained from the microhardness and the diffusivity profile are in close agreement. Since these two parameters reflect different properties of the material, it is not possible to compare directly microhardness and thermal diffusivity. Although a close anti-correlation between microhardness and diffusivity has been found for steel [7, 19], this may not be true for all materials. In fact, the thermal diffusivity profiles seem to be more consistent with the optical micrograph and the TEM results, indicating a more direct relationship between the thermal diffusivity and the microstructure and grain size. A proportionality between the thermal diffusion length and the grain size has been observed before [20]. Sample 2 also shows the drastic improvement in laser processing attained by glass blasting the sample surface before processing. The profile of sample 3 shows that glass blasting itself has affected a layer about 65 μm thick, monotonically reducing the thermal diffusivity, with the maximum reduction being 18% at a depth of 20 μm. Sample 4 gives a non-monotonic thermal diffusivity depth profile which is in close agreement with the microhardness profile and also shows an anti-correlation between hardness and thermal diffusivity. This also proves the ability of our reconstruction algorithm to profile different shapes, as mentioned above, with superior depth resolution to that attained by the conventional microhardness testing, which has the added disadvantage of being destructive.

4. Conclusions

In this paper we have described a reliable non-destructive remote sensing method which allows the reconstruction of thermal diffusivity profiles in an inhomogeneous sample. We have investigated hardened layers of laser-processed Zr–2.5Nb alloy samples, over a range of depths (8–250 μm) limited only by the detection electronics. Although a monotonically increasing diffusivity profile (eqn. (9)) is assumed in the beginning, we have shown that our algorithm can handle arbitrary profiles, owing to the local adjustment of the (α_0,q) values (eqn. (8)), at every experimental frequency.

To improve the power of this technique as a completely quantitative tool for depth profiling of laser-processed samples, it is necessary to relate thermal diffusivity to actual physical changes taking place within the material. Therefore, future work should be directed towards studying the effects on thermal diffusivity of changes in microstructure, grain size, thermal stress, hardness, etc.

Acknowledgments

Partial support of this project by the Natural Sciences and Engineering Research Council of Canada is gratefully acknowledged. One of us (MTC) wishes to thank the Chinese National Commission of Education for granting him research leave, and Ontario Hydro for providing financial assistance, which made this work possible. We would also like to thank Dr K. F. Amouzouvi and his coworkers at Whiteshell Laboratories of AECL, Pinawa, Manitoba, Canada, for the additional data provided by TEM studies.

References

1 K. F. Amouzouvi, L. J. Clegg and R. C. Styles, in S. A. Meguid (ed.), *Surface Engineering*, Elsevier, London, 1990, p. 270.
2 G. P. Sabol, S. G. McDonald, J. I. Nurminen and W. A. Jacobson, in R. B. Adamson and L. F. P. van Swam (eds.), *Zirconium in the Nuclear Industry, Proc. Seventh Int. Symp., ASTM Spec.Tech. Publ., 939* (1987) 168.
3 J. Rawers, W. Reitz, S. Bullard and E. K. Roub, *Corrosion, 47* (Oct. 1991) 769.
4 T. R. Anthony and H. E. Cline, Surface corrosion inhibition of zirconium alloys by laser surface beta-quenching, *US Patent 4294631*, October 13, 1981.
5 M. Munidasa and A. Mandelis, in A. Mandelis (ed.), *Progress in Photoacoustic and Photothermal Science and Technology*, Vol. 1, Elsevier, New York, 1991, pp. 313–344.
6 P.-E. Nordal and S. O. Kanstad, *Phys. Scr., 20* (1979) 659.
7 T. C. Ma, M. Munidasa and A. Mandelis, *J. Appl. Phys., 71* (1992) 6029.
8 B. K. Bein, M. Wojczak and J. Pelzl, *Mater. Sci. Eng., A122* (1989) 93.
9 A. Mandelis and J. D. Lymer, *Appl. Spectrosc., 39* (1985) 473.
10 A. Mandelis, S. B. Peralta and J. Thoen, *J. Appl. Phys., 70* (1991) 1761.
11 A. Mandelis, E. Schoubs, S. B. Peralta and J. Thoen, *J. Appl. Phys., 70* (1991) 1771.
12 T. M. Hiller, M. G. Somekh, S. J. Sheard and D. R. Newcombe, *Mater. Sci. Eng., B5* (1990) 107.

13 P. Cielo, L. A. Utracki and M. Lamontagne, *Can. J. Phys., 64* (1986) 1172.
14 M. G. Dreyfus, *Appl. Opt., 2* (1963) 1113.
15 S. B. Peralta, S. C. Ellis, C. Christofides, A. Mandelis, H. Sang and B. Farahbakhsh, *J. Res. Non-destruct. Eval., 3* (1991) 69.
16 Y. S. Touloukian, R. W. Powell, C. Y. Ho and M. C. Nicolaou (eds.), *Thermophysical Properties of Matter,* Vol. 10, IFI/ Plenum, New York, 1973.
17 H. E. Boyer and T. L. Gall (eds.), *Metals Handbook,* desk edition, American Society of Metals, Metals Park, OH, 1985.
18 W. P. Leung and A. C. Tam, *J. Appl. Phys., 56* (1984) 153.
19 J. Jaarinen and M. Luukkala, *J. Phys. C, 6–44* (1983) 503.
20 A. Rosencwaig, in D. O. Thompson and D. E. Chimenti (eds.), *Review of Progress in Quantitative NDE,* Vol. 9, Plenum, New York, 1990, p. 2031.